High-Resolution X-ray Microtomography for the Detection of Lung Tumors in Living Mice

Nora M. De Clerck, Kris Meurrens†, Horst Weiler‡, Dirk Van Dyck§, Greet Van Houtte*, Piter Terpstra† and Andrei A. Postnov*,§*

*Department of Biomedical Sciences, University of Antwerp, Groenenborgerlaan 171, Antwerp B-2020, Belgium; †PHILIP MORRIS Research Laboratories, Grauwmeer 14, Leuven B-3001, Belgium; ‡PHILIP MORRIS Research Laboratories, Fuggerstrasse 3, Köln D-51149, Germany; §Department of Physics, University of Antwerp, Groenenborgerlaan 171, Antwerp B-2020, Belgium

Abstract

In the present study, the feasibility of applying high-resolution microtomography (micro-CT) for the detection of lung tumors was investigated in live mice at an early and more advanced stage of tumor development. The chest area of anesthesized mice was scanned by X-ray micro-CT. In mice with a minor and heavy tumor load, micro-CT proved to be a fast and noninvasive imaging device for the detection of lung tumors. After validation of the CT data by histologic sectioning, it was shown that the majority of tumors could be distinguished in the reconstructed virtual slices obtained by micro-CT. The data from micro-CT were also confirmed by visual inspection of the inflated and excised lungs postmortem. *In vivo* micro-CT opens broad perspectives for imaging tumor development and its progression in a noninvasive way. Micro-CT also allows for longitudinal evaluation of the treatment of lung cancer by drugs.

Neoplasia (2004) **6**

Keywords: X-ray microtomography, *in vivo* scanning, lung tumors, 3D rendering, urethane.

Introduction

Recently, high-resolution X-ray microtomography (micro-CT) has become a promising technique for imaging the inner anatomy of small laboratory animals [1–3]. The major advantage of micro-CT is that visualization is fully noninvasive. In biomedical research, micro-CT has been applied mainly for studying bones [4,5] and other calcified tissues [6,7].

A new, interesting challenge for X-ray micro-CT is visualization of soft tissues in organs such as the lungs. Previously, analysis of lungs has been reported in humans using clinical CT [8–11]. In small laboratory animals, there is an urgent need for a high-spatial-resolution, noninvasive visualization of the lungs. Therefore, the question was raised as to whether micro-CT can be effective as a diagnostic tool for detecting lung tumors at the earliest possible stage in live mice. Up to now, detection of these tumors has required sacrifice of the mice for histologic examination and/or sectioning and microscopic observation, which are both destructive and time-consuming procedures.

In the present study, live mice suffering from lung tumors, induced by an injection of the carcinogenic agent urethane [12], were studied by X-ray micro-CT.

The diseased lung tissue could be distinguished from normal soft tissue in the micro-CT pictures both at an early stage and a more advanced stage of tumor development. A good correlation was found between data from micro-CT and visual inspection of the excised lungs as well as after microscopic observation of histologic sections. These noninvasive imaging possibilities by micro-CT allow longitudinal studies of tumor development and progression, and open interesting perspectives for the evaluation of drug treatment of lung tumors.

Methods

Animal Model

Three groups of adult A/J mice—one untreated control group and two treated tumor-bearing groups—were studied. Lung tumors were induced by a single intraperitoneal injection (1000 mg/kg bodyweight) of urethane, a carcinogenic agent known to induce lung tumors in A/J mice [12].

One group of 1-year–old mice ($n = 5$), originating from the Jackson Laboratory (Bar Harbor, ME), was treated with urethane and studied 9 months after exposure to urethane. These mice were expected to be suffering from a heavy tumor load. One group of 6-week–old A/J mice from Harlan ($n = 5$) was injected with urethane and examined after a period of 15 weeks of exposure. Small tumors were to be expected. As a control, another group ($n = 5$) of 6-week–old A/J mice was kept for 15 weeks without any treatment.

Care and use of the mice were in accordance with the American Association for Laboratory Animal Science Policy

Address all correspondence to: Nora De Clerck, PhD, Department of Biomedical Sciences, University of Antwerp (RUCA), Groenenborgerlaan 171, Antwerp B-2020, Belgium.
E-mail: nodecle@ruca.ua.ac.be
Received 4 December 2003; Revised 6 February 2004; Accepted 11 February 2004.

(1991). The animal experiments were previously approved by the IACUC.

Scanning Procedure

All animals were anesthesized by an intramuscular injection (average dose, 8 ml/kg) of a mixture of ketaminium hydrochloridum and xylazine hydrochloridum diluted with saline (2.1 ml of 50 mg/ml Ketalar [Parke-Davis], 0.3 ml of 2% Rompun [Bayer], and 3.4 ml of 0.9% NaCl). This protocol provided good anesthesia during the whole scanning period. The mice were placed on their back on an animal bed. The interpretation of the images was enabled by the fact that the animals were always lying in a more or less similar position. Banding of the chest area proved important to reduce movement artifacts. A nonelastic kind of paper tape, with a protection for the fur, was used. Banding was not so tight that it might impair normal respiration. This banding resulted in a change in the geometry of thorax movement and reduced the amplitude of the movement of the ribs within the scanning area. Care was taken to keep the mice warm during recovery from anesthesia after scanning.

For scanning, a new *in vivo* X-ray micro-CT system was used (Skyscan 1076; Skyscan, Aartselaar, Belgium) without gating for cardiac or respiratory motion. Both the X-ray source (focal spot size, 5 μm; energy range, 20–100 keV) and the detector (CCD camera, 2.3 × 4 k) rotated around the animal. The scanner had three different fields of view: 18, 36, and 66 mm. Scans were isotropic and a voxel size of 35 × 35 × 35 μm was chosen to have an exposure time of 17 minutes per scan. Virtual cross sections were reconstructed by the cone beam algorithm of Feldkamp et al. [13]. Further technical details about the scanner have been published elsewhere [15].

Preparation of the Lungs

After scanning, the animals were sacrificed for pathomorphologic examination.

The lungs were manually instilled with, and subsequently kept in, Tellyesniczky solution. Fixation in Tellyesniczky solution renders the normal lung tissue transparent, allowing macroscopic visualization of tumor nodules without compromising further histopathologic examination. After 2 days, the lungs were transferred and stored into a solution of 70% ethanol. Digital pictures were taken of the lungs of all mice.

Histologic Sections

To correlate the results obtained by micro-CT scanning and macroscopic pathologic–anatomic examination of the lungs after fixation, on one hand, and the results of histopathologic examination, on the other hand, two representative pairs of lungs, one from each age group, were chosen for further detailed histopathologic routine processing with paraplast embedding. The left and right lungs of each animal were embedded individually in a "standing" position so that transaxial cross sections could be taken every 100 μm throughout the whole paraplast block. Histopathologic examination and image documentation were performed on hematoxylin and eosin (H&E)–stained slides.

Results

Soft tissues in the lungs in mice could be clearly visualized by X-ray micro-CT. Figure 1 shows the results of scanning the chest area of a healthy live mouse. On the scout view (X-ray shadow view, panel A), the region to be scanned and the specific cross section could be chosen. In panel B, a reconstruction of the selected cross section is illustrated: the anatomic structures of the chest including bones, muscles, and soft tissues in organs can be distinguished clearly. Some noise was inevitably due to movement artifacts.

Banding of the chest area proved useful to reduce these motion artifacts. This was illustrated in Figure 2*a* where a cross section through the same heart–lung region is shown after banding the chest area in a living mouse.

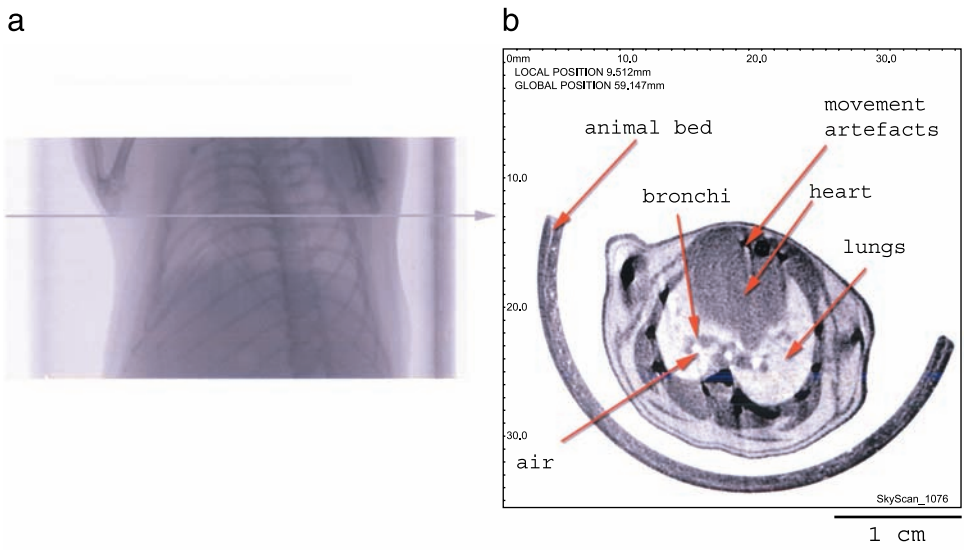

Figure 1. *Panel (a): Scout view through the chest area of a live healthy mouse. The horizontal line indicates where the virtual cross section was located. Panel (b): Reconstructed virtual cross section. Notice the lungs and the heart. Distinction could be made between the lung tissue, bronchi, and empty air spaces.*

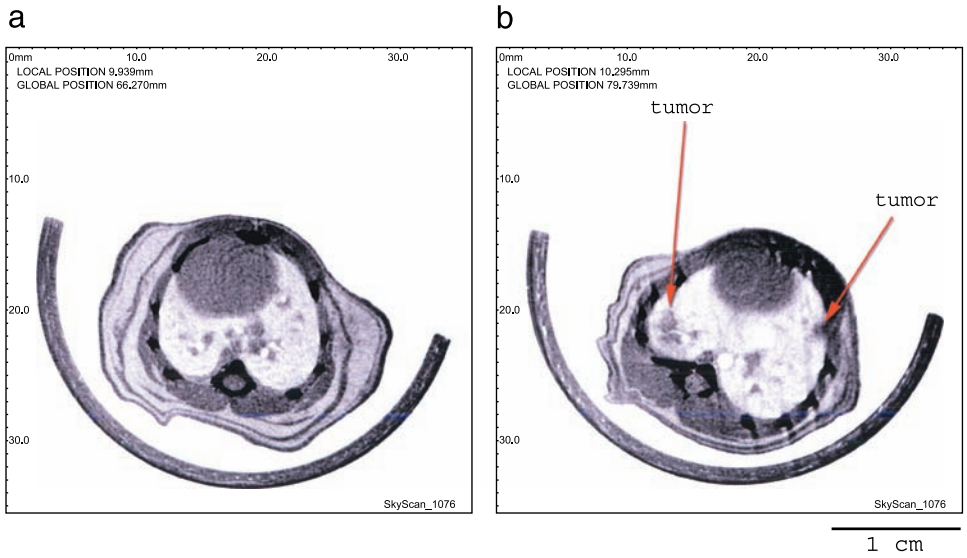

Figure 2. *(a) Reconstructed cross section through the chest area of mouse. In panel (a), special banding was applied to reduce motion artifacts. Panel (b) illustrates a representative virtual cross section through the lungs of a representative mouse with heavy tumor load (10 months after injection). The arrows indicate two representative tumors.*

In a first series of experiments, a group of older mice (n = 5) with a heavy tumor load was scanned. At this age, a massive development of tumors was to be expected. Figure 2*b* shows a representative virtual cross section through the chest area of one of these animals. Several tumors can be observed as denser parts in the reconstructions.

After micro-CT analysis, the animals were sacrificed under anesthesia and the lungs were instilled and photographed. Figure 3 shows a picture of a representative pair of lungs where the tumors can be observed macroscopically. The absolute number of tumors or nodules was higher in the right lung than in the left lung. A good visual correlation could be found between the appearance and dimensions of the tumors visible in the virtual CT slices and in the macroscopic pictures of the lungs. This is summarized in Figure 3 by inserting CT cross sections through the corresponding tumor. Out of the 15 tumors visible on the digital photo, 14 tumors could be localized in the scans. This result was obtained independently from two observers at two different times and was repeated in five mice. However, in the virtual slices from the CT, it proved more difficult to localize the tumors at the hilus of the lung or at the periphery. Micro-CT analysis of the virtual cross sections was performed prior to the macroscopic inspection of the photographs of the excised lungs.

As a validation, the representative pair of lungs in Figure 3 was sectioned every 100 μm and stained for histologic examination. In Figure 3*b*, histologic cross sections were illustrated with reference (number) to each tumor. Histopathologic examination showed that all tumors detected by micro-CT were indeed neoplastic alterations. No scar tissue, microgranulomas, or hyperplastic lymphocellular follicles were observed.

There proved to be a good correlation between macroscopic visual information, CT images, and histologic slicing even though there were a few very small tumors seen in histologic slides that were not detected by micro-CT.

A second and more challenging question was whether tumor development in an earlier stage could also be detected by micro-CT. Therefore, a second series of mice was scanned and prepared for further investigation. In these mice, the tumor load was less and the tumors were smaller in diameter. As illustrated in Figure 4, these smaller tumors could be discovered by micro-CT. Similar to Figure 3, the lungs were excised after scanning, instilled, and photographed. Again a positive visual correlation was made between the reconstructed CT scans and the macroscopic and microscopic information, as shown in Figure 4*a*. Histopathologic examination confirmed that all tumors detected by micro-CT were indeed neoplastic changes.

As an additional result, a three-dimensional (3D) model (Figure 4*b*) was reconstructed for this lung. The reconstruction is semitransparent for optimal visualization of the tumors. The spatial orientation and correlation of the tumor spots become more evident.

Discussion

In the present report, it is shown that major anatomic structures such as the lungs, heart, larger blood vessels in lungs, and the ribs can be recognized distinctively in the virtual cross sections reconstructed after micro-CT scanning. The fact that it proved possible to reconstruct virtual cross sections through the chest area despite cardiac and respiratory movement is an important achievement. The reconstructions of the virtual cross sections were of good quality in spite of some movement artifacts. Imaging of the soft tissues in the lungs of living mice with high-resolution micro-CT proved to be possible, notwithstanding the small differences in density between tissues present in lung.

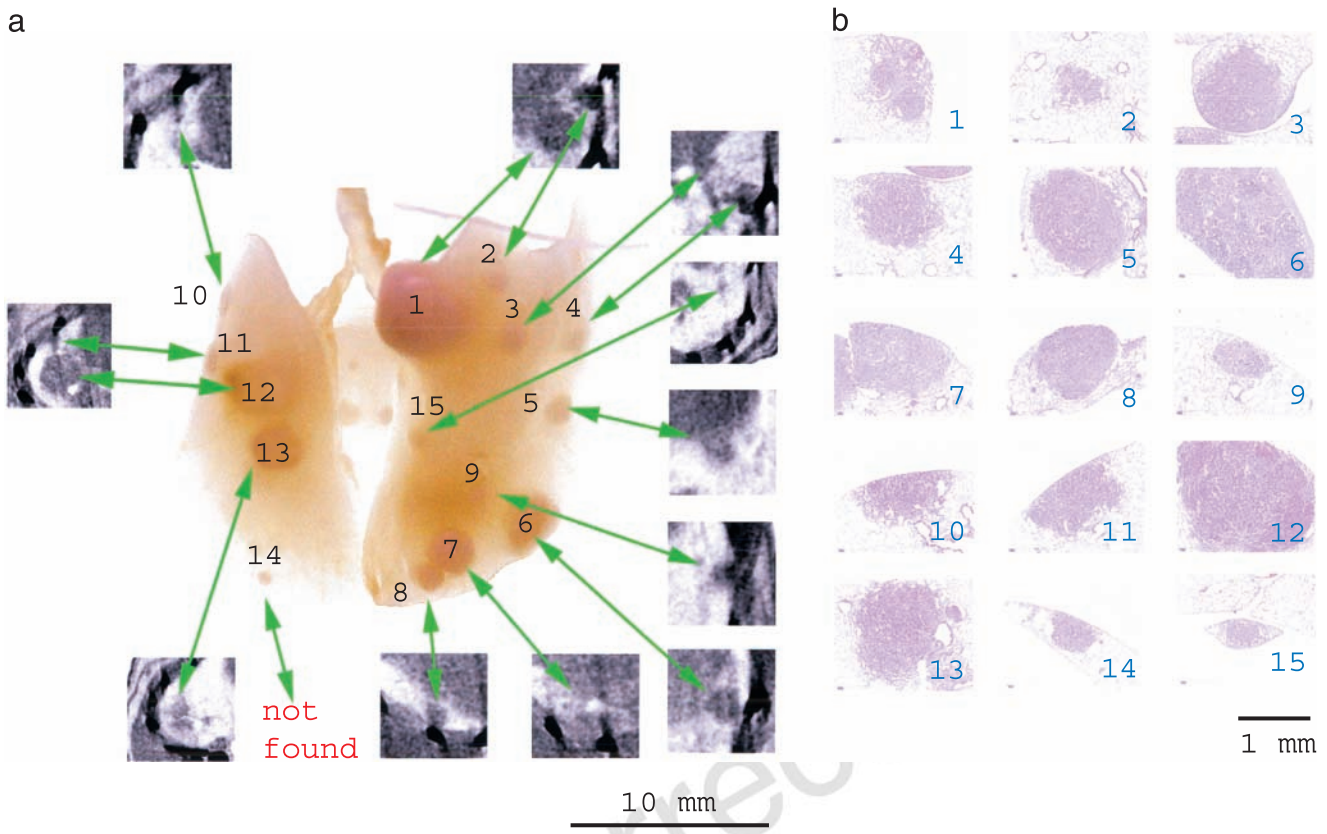

Figure 3. *(a) Photograph of the excised and inflated pair of lungs of a representative mouse with heavy tumor load. The tumors are numbered. The virtual in vivo micro-CT cross sections through each tumor were superimposed. (b) Shows the identification of each tumor after histologic staining. In the two lobes shown in the picture of this representative example, a total of 15 tumor regions was recognized. Tumor 14 was not found in the micro-CT cross sections.*

The most important result in this study is the observation that tumor tissue can be distinguished from healthy tissue in a mouse model with induced tumor load. Tumor tissue in lungs could be detected with high reliability and low radiation dose. Nevertheless, tumors and blood vessels in lungs have a similar X-ray absorption and care should be taken not to confuse them.

These observations are in line with a previous report [15] where micro-CT was applied successfully to detect tumors. In comparison to this study, the spatial resolution

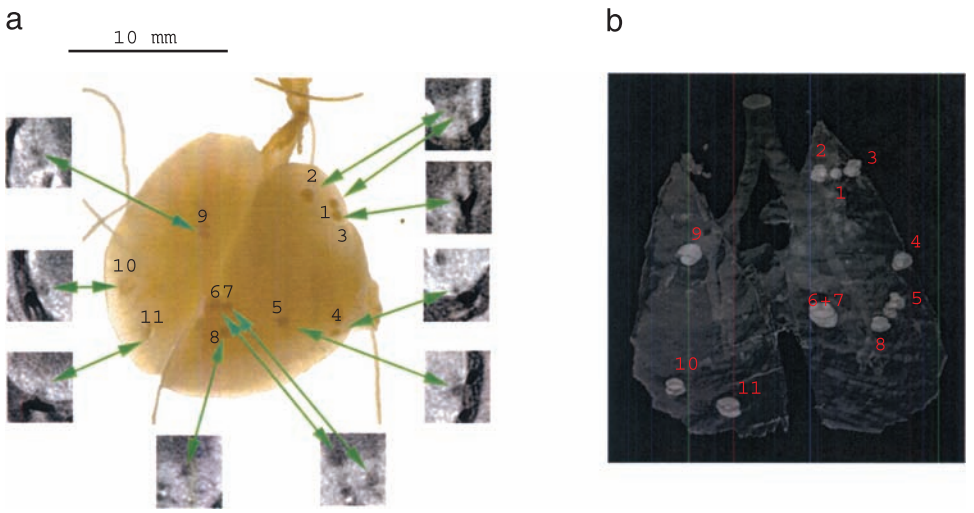

Figure 4. *(a) Photograph of the excised and inflated lungs of a representative mouse with minor tumor load. The tumors were numbered. The cross sections by in vivo micro-CT were indicated on the picture. (b) Semitransparent 3D reconstruction of the same lung with minor tumor load, based on the virtual in vivo CT slices. The spatial organization and localization of the tumor spots can be seen.*

Q4

was doubled (voxel size 35 × 35 × 35 μm) in our experiments. The scanner used in our experiment can provide up to 9 μm pixel size (hence, approximately 15 μm resolution). However, true resolution depends on scanning material and exposure time. When the exposure time is diminished to reduce the radiation dose for the animal, signal-to-noise ratio also declines together with the resolution. Moreover, unavoidable movement artifacts from animal breathing and internal organ movement are always present and do not allow achievement of the highest possible resolution. The compromise between spatial resolution and dose required to obtain this given resolution in living animals, especially in soft tissues, should always be respected.

Dose load applied in the experiment was 0.4 Gy/15 min for a mouse scan. This dose allows to distinguish tumors and blood vessels in the lungs, together with separate lung tissues and empty spaces filled with air. This is promising in the study of diseases where lung tissue can vary in density, such as emphysema [8].

However, in the present study, the effect of dose level itself on tumor development was not studied. The animals were scanned only once, and then sacrificed for lung preparation and histology. The effect of X-ray dose on carcinogenesis in lungs may be an interesting topic for a future study.

Another reason for reducing the scanning time was the relatively weak condition of the elder mice. Banding of the chest area reduced the movement artifact. An additional important reduction of movement was due to the fact that the mice were lying on their back on the animal bed while being scanned.

Scanning in the present report was isotropic, which made it possible to reconstruct a 3D model of the lung. 3D models enable faster spatial correlation with visual and histopathologic controls.

In addition, the animal model in the present study was unique as tumor development was caused by a simple injection of a carcinogenic agent and did not require the implantation of tumor tissue in mice. This model proved to be more representative of tumor development after environmental exposure to carcinogens [12,16,17].

To validate the observations by micro-CT, all the lungs were excised, instilled, and photographed. On the picture, the tumors could be seen macroscopically. Two independent observers correlated the incidence of the tumors in the virtual cross sections. Most of the tumors could be recognized in the virtual slices; however, it turned out to be more difficult to observe the tumors at the periphery of the lungs and at the hilus. Yet, some additional tiny tumors, which were not detected by micro-CT, could be revealed by histology.

An accurate estimate of the actual resolution of micro-CT is only possible for motionless objects, which is not the case in these *in vivo* experiments. In the scans, the actual movement in every part of the cross section is not known. In the heart region, tissue motions are much more pronounced than those closer to the vertebral column. As a result, some of the tumors may become blurred and look larger than their actual size. In the present scanning conditions, we can estimate that the smallest tumor size detected was approximately 200 μm.

Our results refer to a visual correlation because from our experience, it became obvious that measurements of tumor size or tumor volume in a living and breathing lung are not straightforward analyses. As discussed above, contours and shapes may become distorted by movement artifacts. That is the reason why no quantitative correlation between the different imaging techniques was made. Nevertheless, a good visual correlation between spot size in the cross sections and the histologic slices was evident.

Consequently, our results show that micro-CT is a useful tool for initial screening, mainly because it is noninvasive. Another advantage is that imaging is relatively fast for scanning and reconstructing (17-minute scan, 40-minute reconstruction time). Visualization by micro-CT avoids technical processing of tissues in histopathology. A major drawback of the classic histologic techniques is the interference of shrinkage, the extent of which cannot be quantified.

Although nuclear magnetic resonance (NMR) proved more suitable for imaging soft tissues in live animals [18], the pictures obtained in preliminary experiments were completely blurred by motion artifacts. This confirmed the previous observation [15] that NMR is not useful for imaging the chest area of living animals, unless special adaptations such as respiratory gating and so on are implemented in the future. In comparison to NMR, imaging with micro-CT is faster and less expensive. This is interesting for phenotyping larger numbers of animals. Moreover, micro-CT has a higher spatial resolution than NMR.

Injection of contrast agents containing iodine did not help distinguish between vessels and tumors in the lungs in the virtual cross sections. It may prove more appropriate for increasing the contrast in other organs such as the heart and the kidneys. However, the experiments with contrast agents were restricted to feasibility experiments, as injection of contrast agents represented a serious additional stress for the diseased mice.

An interesting future development to increase the resolution of *in vivo* scanning of lungs would be the implementation of a synchronization between image acquisition and respiratory and cardiac frequencies in the animals. This would not only reduce the motion artifacts but would also contribute to the increase in resolution that can be obtained in the scans. Another interesting improvement for scanning would be the possibility to acquire images at a higher resolution. For this latter issue, either dose should be increased, or a more sensitive detector should be used. Another important challenge is to reduce the artifacts near the bones when the bones are screening the surrounding tissues. This is mainly a problem of the reconstruction algorithm.

Conclusions

These findings open, wide perspectives for the application of micro-CT as a diagnostic tool for the detection of early and advanced stages in tumor development in lung tissues in living mice. The major advantage of micro-CT is that it is

fully noninvasive. Therefore, micro-CT can be applied successfully for long-term studies of growth, development, and drug treatment of lung tumors in mice, and for reducing the number of mice in carcinogenicity studies.

References

[1] Paulus MJ, Gleason SS, Kennel SJ, Hunsicker PR, and Johnson DK (2000). High resolution X-ray computed tomography: an emerging tool for small animal cancer research. *Neoplasia* **2** (1,2), 62–70.

[2] De Clerck NM, Van Dyck D, and Postnov AA (2003). Non-invasive high-resolution μCT of the inner structure of living animals. *Microsc Anal* **81,** 13–15.

[3] Boyde A, De Clerck NM, and Sasov A (2000). MicroCT of bones and soft tissues. *Microsc Anal (UK Ed)* **76,** 70.

[4] Postnov AA, Vinogradov A, Van Dyck D, Saveliev SV, and De Clerck NM (2003). Quantitative analysis of bone mineral content by X-ray microtomography. *Physiol Meas* **24** (1), 165–178.

[5] Waarsing JH, Day JS, van der Linde JC, Ederveen AG, Spanjers C, De Clerck NM, Sasov A, and Weinans H (2003). Detecting and tracking local changes in the tibiae of individual rats: a novel method to analyse longitudinal *in vivo* micro-CT data. *Bone* XX, X—XX (in press).

[6] Postnov AA, De Clerck NM, Sasov A, and Van Dyck D (2002). 3D *in vivo* X-ray microtomography of living snails. *J Microsc* **205** (2), 201–205 (2002 plus cover illustration of the issue).

[7] Postnov AA, Van Dyck D, Saveliev S, Saso A, and De Clerck NM (2002). Definition of local density in biological calcified tissues using X-ray microtomography. Progress in biomedical optics and imaging. *Proc SPIE* **3** (19), 749–755.

[8] Gould G, MacNee W, McLean A, Warren P, Redpath A, Best J, Lamb D, and Flenley D (1988). CT measurement of lung density in life can quantitate distal airspace enlargement—an essential defining feature of human emphysema. *Am Rev Respir Dis* **137,** 380–391.

[9] Biernacki W, Redpath AT, Best JK, and MacNee W (1997). Measurement of CT lung density in patients with chronic asthma. *Eur Respir J* **10,** 2455–2459.

[10] Takasugi JE and Godwin D (1998). Radiology of chronic obstructive pulmonary disease. *Radiol Clin North Am* **36** (1), 29–55.

[11] Webb WR, Gatsonis C, Zerhouni EA, Heelan RT, Glazer GM, Francis IR, and McNeil BJ (1991). CT and MR imaging in staging non-small cell bronchogenic carcinoma: report of the radiologic diagnostic oncology group. *Thorac Radiol* **178,** 705–713.

[12] Stoner G (1991). Lung tumors in strain A mice as a bioassay for carcinogenicity of environmental chemicals. *Exp Lung Res* **17,** 405–423.

[13] Feldkamp LA, Davis LC, and Kress JW (1984). Practical cone-beam algorithm. *J Opt Soc Am, A* **1** (6), 612–619.

[14] www.skyscan.be

[15] Kennell SJ, Davis IA, Branning J, Pan HP, Kabalka GW, and Paulus MJ (2000). High resolution computer tomography and MRI for lung tumor growth in mice undergoing radioimmunotherapy: correlation with histology. *Med Phys* **27** (5), 1101–1107.

[16] Stoner GD, Greisiger EA, Schut HAJ, Pereirea MA, Loeb TR, Klaunig JE, and Branstetter DG (1984). A comparison of the lung adenoma response in strain A/J mice after intraperitoneal and oral administration of carcinogens. *Toxicol Appl Pharmacol* **72,** 313–323.

[17] Witschi H and Doherty D (1984). Butylated hydroxyanisole and lung tumor development in A/J mice. *Fundam Appl Toxicol* **4,** 795–801.

[18] Hoogenraad CC, Koekkoek AB, Akhmanova H, Krugers B, Dortland M, Miedema A, van Alphen W, Kistler M, Jaegle M, Koutsourakis N, Van Camp M, Verhoye A, Van der Linden I, Kaverina F, Grosveld CI, and De Zeeuw N (2002). Targeted mutation of Cyln2 in the Williams syndrome critical region links CLIP-115 haploinsufficiency to neurodevelopmental abnormalities in mice. *Nat Genet* **32,** 116–127.